

Boise State University

ScholarWorks

---

Geosciences Faculty Publications and  
Presentations

Department of Geosciences

---

2-20-2020

## Constraints on the Shallow Deformation Around the Main Frontal Thrust in Central Nepal from Refraction Velocities

Yixiang Liu

*Nanyang Technological University*

Judith Hubbard

*Nanyang Technological University*

Rafael V. Almeida

*Nanyang Technological University*

Anna Foster

*Nanyang Technological University*

Lee Liberty

*Boise State University*

*See next page for additional authors*

---

### Publication Information

Liu, Yixiang; Hubbard, Judith; Almeida, Rafael V.; Foster, Anna; Liberty, Lee; Lee, Ying Sin; and Sapkota, Soma Nath. (2020). "Constraints on the Shallow Deformation Around the Main Frontal Thrust in Central Nepal from Refraction Velocities". *Tectonophysics*, 777, 228366-1 - 228366-10. <https://doi.org/10.1016/j.tecto.2020.228366>

---

**Authors**

Yixiang Liu, Judith Hubbard, Rafael V. Almeida, Anna Foster, Lee Liberty, Ying Sin Lee, and Soma Nath Sapkota



## Constraints on the shallow deformation around the Main Frontal Thrust in central Nepal from refraction velocities

Yixiang Liu<sup>a</sup>, Judith Hubbard<sup>a,b,\*</sup>, Rafael V. Almeida<sup>b,f</sup>, Anna Foster<sup>b,c,f</sup>, Lee Liberty<sup>d</sup>, Ying Sin Lee<sup>b</sup>, Soma Nath Sapkota<sup>e</sup>

<sup>a</sup> Asian School of the Environment, 50 Nanyang Ave., Nanyang Technological University, 639798 Singapore, Singapore

<sup>b</sup> Earth Observatory of Singapore, 50 Nanyang Ave., Nanyang Technological University, 639798 Singapore, Singapore

<sup>c</sup> Département des sciences de la Terre et de l'atmosphère, Université du Québec à Montréal, Canada

<sup>d</sup> Department of Geosciences, Boise State University, ID, USA

<sup>e</sup> Department of Mines and Geology, Kathmandu 44600, Nepal

<sup>f</sup> School of Earth Science, Energy and Environment, Yachay Tech University, Ecuador.

### ARTICLE INFO

#### Keywords:

P-wave velocity  
Seismic refraction  
Nepal Himalaya  
Sediment thickness  
Water table  
Main Frontal Thrust

### ABSTRACT

The youngest fault system in the Himalayan orogeny is the Main Frontal Thrust (MFT), the frontal ramp of the Main Himalayan Thrust, which is expected to host the largest and most damaging earthquakes in Nepal. We characterize the upper few hundred meters below the surface across two MFT fault strands using ten high-resolution seismic profiles that we acquired in 2014 and 2015 with a 6-tonne Vibroseis source. We use first arrival picks from 625,416 seismic traces to derive P-wave seismic velocity models using a wavepath eikonal traveltimes inversion method, and derive estimates of alluvium thickness and water table depth across these faults (the Patu and Bardibas thrusts), allowing us to constrain the subsurface geometry of the MFT.

Our results show that 1) seismic velocities range from 255 to 3660 m/s, consistent with dry and saturated alluvium, and Siwalik bedrock; 2) low-velocity alluvium varies between ~20–50 and ~80–120 m thick in the hanging wall and footwall of the Bardibas thrust, respectively, corresponding to ~60–70 m of uplift of the hanging wall since deposition; 3) the two thrusts are soft-linked, and the western tip of the Bardibas thrust lies ~6 km west of its surface expression; 4) during the dry season, the water table is ~25–100 m higher in the hanging walls of the faults than in their footwalls, due to the larger thickness of permeable alluvium in the footwalls, and the water table shallows towards the east in the hanging wall of the Bardibas thrust; and 5) consistent with previous studies, the Patu thrust breaches the surface, while the Bardibas thrust is blind at Ratu Khola. These results also demonstrate that it should be possible to constrain the rate of uplift above the Bardibas thrust by drilling and dating sediments on both sides, which would complement existing measurements from terrace uplift.

### 1. Introduction

The Main Himalayan Thrust (MHT) is the largest and fastest-slipping continental megathrust on Earth (Davies and Brune, 1971). This fault system is the result of the collision of the Indian and Eurasian plates, which started at ~50 Ma (Aitchison et al., 2007; Khan et al., 2009; Bouilhol et al., 2013) and continues today with a convergence rate of 17–21 mm per year (Larson et al., 1999; Ader et al., 2012). This convergence is accommodated by large and great earthquakes, and poses a significant seismic hazard to the hundreds of millions of people living in the Ganges plain and Himalayan foothills.

The Main Frontal Thrust (MFT) represents the southernmost and most active surface-rupturing fault associated with this megathrust. Because this is the only part of the system that has a direct surface expression and is known to be active, it has been the target of numerous paleoseismic studies aimed at understanding the surface and near-surface deformation associated with past slip events. During the dry seasons of 2014 and 2015, we explored the subsurface geometry and deformation associated with the MFT in order to link the deeper geometry of the fault with its surface expression, by acquiring active source seismic data with a 6-tonne Vibroseis source. As part of this project, we collected 20 high-resolution seismic reflection profiles across the MFT

\* Corresponding author at: Asian School of the Environment, 50 Nanyang Ave., Nanyang Technological University, 639798 Singapore, Singapore  
E-mail addresses: [jhubbard@ntu.edu.sg](mailto:jhubbard@ntu.edu.sg) (J. Hubbard), [ralmeida@yachaytech.edu.ec](mailto:ralmeida@yachaytech.edu.ec) (R.V. Almeida), [lliberty@boisestate.edu](mailto:lliberty@boisestate.edu) (L. Liberty), [leey@ntu.edu.sg](mailto:leey@ntu.edu.sg) (Y.S. Lee).

<https://doi.org/10.1016/j.tecto.2020.228366>

Received 10 December 2018; Received in revised form 6 January 2020; Accepted 30 January 2020

Available online 01 February 2020

0040-1951/ © 2020 The Authors. Published by Elsevier B.V. This is an open access article under the CC BY-NC-ND license (<http://creativecommons.org/licenses/by-nc-nd/4.0/>).

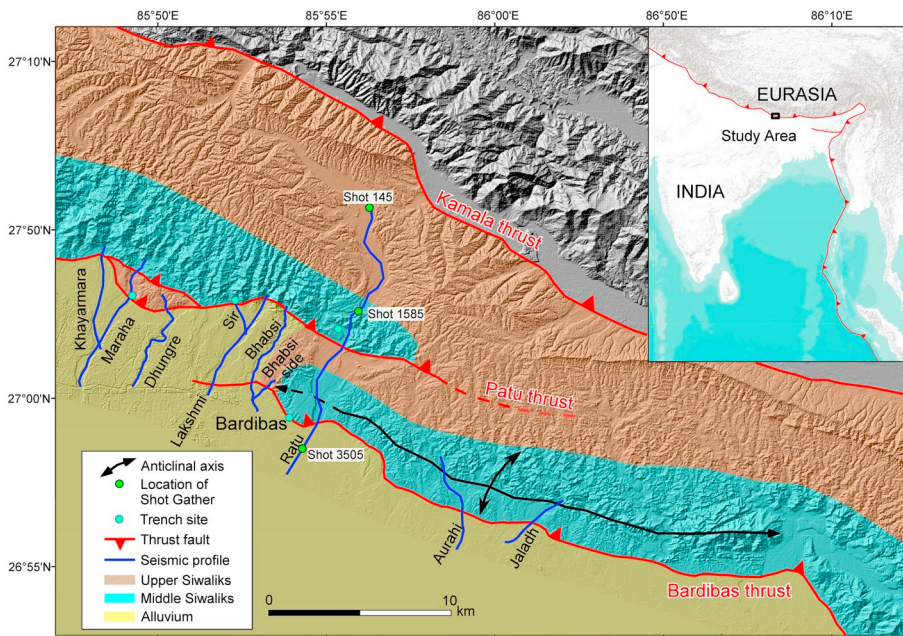


**Fig. 1.** Map of the study area in central Nepal, with 10 seismic transects, superimposed on the geology. The rocks in the study area consist of the mid-Miocene to Pleistocene Siwaliks Group (alternating layers of sandstones and siltstones/mudstones). The MFT in this area has two fault strands: the northern Patu thrust, and the southern Bardibas thrust. Additional thrusts deform the Siwaliks group to the northeast, including the Kamala thrust (shown here).

in central to eastern Nepal, which extend down to ~2 km (Almeida et al., 2018). In this study, we use the first arrivals in our shot gathers to generate high-resolution two-dimensional P-wave velocity models of the upper 200 to 500 m.

Here we use a subset of the full dataset: ten profiles from central Nepal, taken across a step-over in the surface expression of the MFT (see Fig. 1 for locations). The youngest strata in this region consist of Quaternary unconsolidated fluvial sediments deposited above the Neogene Siwalik Group (Dhital, 2016). The Siwalik group consists of fluvial and alluvial strata deposited in the foreland basin of the Himalayas, and lithologically it consists of alternating layers of sandstone and siltstone/mudstone. Our lines capture two fault strands of the MFT that overlap across a right-step: the northern Patu thrust and the

southern Bardibas thrust (Fig. 1). Both thrusts sole into the MHT at ~2 km below the surface (Almeida et al., 2018; Fig. 2A).

Several studies have found evidence of surface ruptures in the area associated with earthquakes. Lave et al. (2005) interpreted a surface rupture at Maraha Khola (“khola” is Nepali for “stream”; Fig. 1) to have formed during an earthquake in ~A.D. 1100. Sapkota et al. (2013) and Bollinger et al. (2014) established that at Sir Khola and Ratu Khola (Fig. 1), the last two great earthquakes in east/central Nepal (A.D. 1255 and 1934) ruptured the surface along the Patu thrust. More recently, Almeida et al. (2018) used a seismic reflection profile along Ratu Khola to show that while the Patu thrust breaches the surface, the Bardibas thrust is blind at this location (Fig. 2A). Almeida et al. further characterize the folding associated with both of these structures, showing

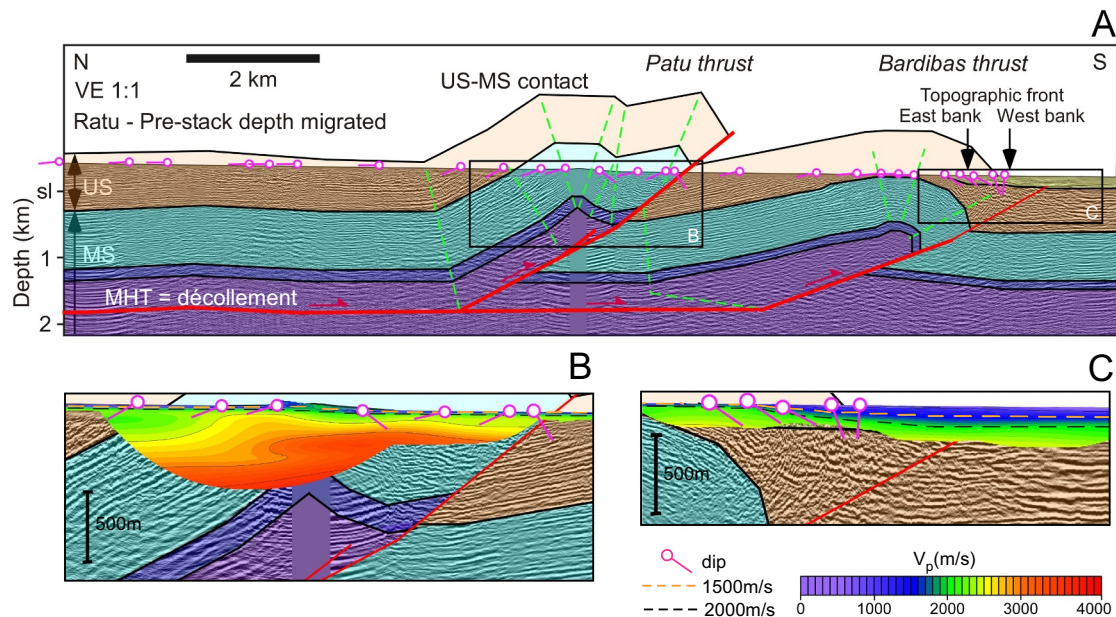


**Fig. 2.** (A) Interpreted seismic reflection profile from the Ratu river (Almeida et al., 2018); see Fig. 1 for location, which is coincident with the Ratu refraction profile presented here. Contact between Upper Siwaliks (US) and Middle Siwaliks (MS) and dip measurements are observed in the field. The décollement (MHT) lies ~2 km below the surface. (B) Close-up of the refraction velocity models at the Patu thrust. The higher velocity rocks are uplifted by the Patu thrust. (C) Close-up of the refraction velocity model at the Bardibas thrust. The rocks here have lower velocities than those in the hanging wall of the Patu thrust.

that slip on the Patu thrust has created a fault bend fold, while slip on the Bardibas thrust has resulted in a  $\sim 4$  km wide, pure-shear anticline (Figs. 1 and 2A).

However, existing studies do not have robust coverage in the few hundred meters below the surface. Lave et al. (2005), Sapkota et al. (2013), and Bollinger et al. (2014) look only at the shallowest few meters, while Almeida et al. cannot fully characterize the upper hundred meters well because of coarse source/receiver spacing relative to imaging depths within their reflection data, especially in complex structural areas (such as near the tip of the Bardibas thrust). Here, our refraction velocities bridge this gap, providing a subsurface view that is between the meter-scale observations of trenches and the kilometer-scale observations of the seismic reflection profiles. Specifically, we look at changes in velocity structure to pinpoint fault strand locations and estimate minimum fault throw (i.e. the vertical component of displacement across a fault). These results are valuable not just for understanding the tectonic deformation of the area, but also provide a window into the way in which the MFT affects groundwater resources in this densely populated region.

## 2. Methods

### 2.1. Data

The seismic data were acquired using a 6-tonne Vibroseis source (an IVI minibuggy) in a split-spread configuration with a 264-channel seismograph (iSeis DAQ III wireless system) with 10 Hz geophones. Source and receiver locations were spaced every 5 m, resulting in a maximum offset of  $\sim 700$  m, except at the beginning and end of each line where the maximum offsets reach  $\sim 1.3$  km. At each source point, data recorded from 6 to 12 linear frequency sweeps of 10–120 Hz were cross-correlated with the theoretical sweep and vertically stacked. The profiles, which range in length from 1.6 to 16.8 km, were acquired along ephemeral riverbeds during the local dry season in 2014 (January–March, November) and 2015 (January–March). We used a standard processing approach to examine the vibroseis records (e.g. Yilmaz, 2001). As the cross-correlation of Vibroseis data produces zero-phase data, we picked the first peak amplitude of the direct or refracted arrivals, rather than the first motions (Fig. 3). This approach resulted in higher pick confidence compared to side lobe picks or phase shifting the data. We estimate our picking uncertainty as a quarter of a wavelength of the  $\sim 70$  Hz central frequency of the head wave, or approximately 3.5 ms. Our approach may be less accurate for the shallowest velocities, but should not significantly alter deeper velocity structures or boundary depths. We manually picked the first peak amplitude every 5th shot using SeisSpace, a seismic processing software. A total of 2369 shots and 625,416 traces were analyzed.

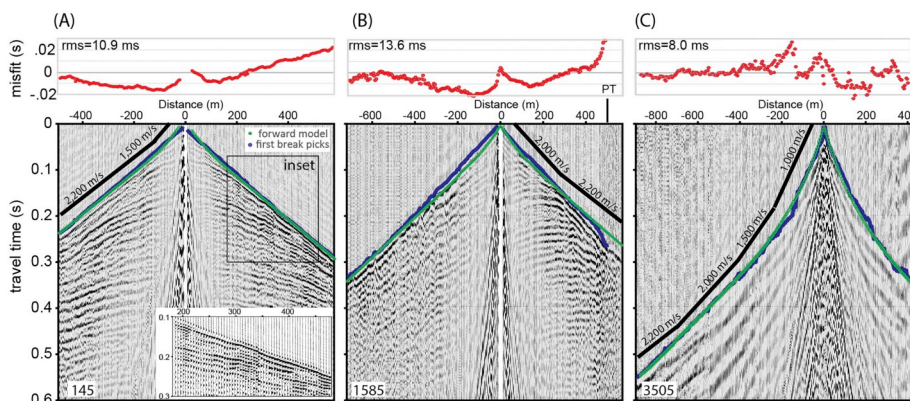


**Fig. 3.** Three examples of shot gathers (145, 1585, and 3505) from the Ratu River profile; locations for each shot are shown in Fig. 1. Changes in data quality and velocity (straight line approximations in black) are evident from north to south. First-break picks and predicted arrivals based on the final velocity model typically agree, as shown by the misfit above each gather. One exception can be noted on the right side of shot 1585; as waves cross the Patu Thrust (PT) the velocity sharply decreases, a feature which is smoothed in the tomography model. Shot coordinates are: 145 (27.095934, 85.937402), 1585 (27.043252, 85.932418), 3505 (26.971991, 85.904706).

### 2.2. Seismic Tomography

We projected the source and receiver locations onto a straight line, and used the traveltimes of the first arrival waves to generate 2D velocity models (Fig. 5; Supplementary Data) in Rayfract (Intelligent Resources, Inc.). This software uses a wavepath eikonal traveltime (WET) method to invert P-wave traveltimes for subsurface P-wave velocities (Schuster and Quintus-Bosz, 1993; Sheehan et al., 2005). With this method, a 1D initial model was obtained automatically from the traveltimes and extended to produce a smooth 2D initial model. The optimum grid size is automatically determined by path coverage, and ranges from 3 to 6 m. We then iteratively refined this initial model between 20 and 100 times (exact grid size and number of iterations for each profile are given in the Supplementary Data), by (1) forward modeling both the ray paths and the traveltimes using the WET method, an Eikonal solver with sensitivity over a Fresnel volume, (2) calculating the traveltime residuals for that model, (3) calculating the source weighting function, and (4) updating the model. The central Ricker wavelet frequency for the WET method was 50 Hz. This method is computationally efficient, and accounts for the band-limited source, diffraction and shadow effects. However, like most tomographic methods, the inversion smooths sharp boundaries and may not preserve small-scale velocity structure or sharp contrasts in velocities produced by faulting (Schuster and Quintus-Bosz, 1993; Jansen, 2011). The final root-mean-square (RMS) error for each profile ranged from 10 to 16 ms; exact values are given in the Supplementary Data.

## 3. Results

The ray path densities (Fig. 4) that correspond to the final velocity model for each of the lines (Fig. 5) show variable depth penetration of  $\sim 100$ – $500$  m, with typical penetration of  $\sim 200$  m. We use our resulting velocity tomograms in two ways. First, we produce generalized velocity-depth curves (Fig. 6) for different stratigraphic sections by spatially averaging our results, which can be used as a baseline for future tomographic or site response studies. Second, we interpret the changes in velocity along the profiles in the context of tectonic deformation, and use the spaced set of 2D lines to assess changes in deformation.

In our first step, we generate three distinct velocity-depth curves for different locations and inferred materials along the profiles: (1) the undeformed fluvial sediment/alluvium south of the Bardibas thrust (i.e. materials not in the hanging wall of any fault; Fig. 6A), (2) the Siwaliks and alluvium in the hanging wall of the Patu thrust (Fig. 6B), and (3) the Siwaliks and alluvium in the hanging wall of the Bardibas thrust and the footwall of the Patu thrust (Fig. 6C) (see Almeida et al., 2018 for further description of these units). We distinguish the latter two because the two faults exhibit different amounts of slip, and our field

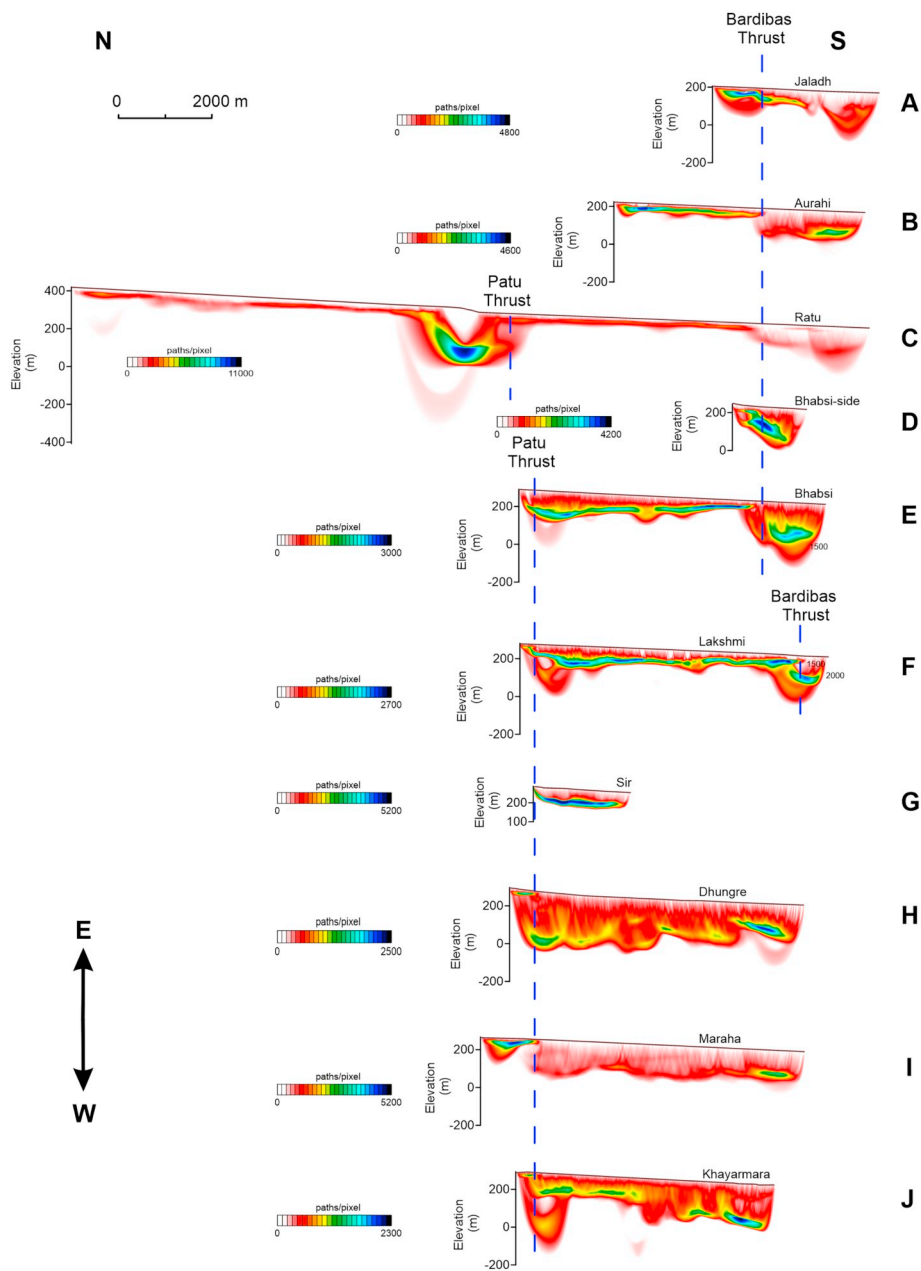


**Fig. 4.** Ray path density for each of the ten rivers (vertical exaggeration = 4:1; vertical scale is depth in meters). Coverage varies both spatially and with depth. Locations are shown in Fig. 1. (A) Jaladh (B) Aurahi (C) Ratu (D) Bhabsi-side (E) Bhabsi (F) Lakshmi (G) Sir (H) Dhungre (I) Maraha (J) Khayarmara. The vertical dashed blue lines represent the locations of the tips of Patu and Bardibas thrusts; the sections are shifted so that these line up with each other. (For interpretation of the references to color in this figure legend, the reader is referred to the web version of this article.)

observations and the mapped geology show that they expose different stratigraphic levels of the Siwaliks.

In the absence of fluids, seismic velocities in fluvial sediments typically increase with depth due to decreasing porosity and according to a power law relationship (e.g., Faust, 1951; Eberhart-Phillips et al., 1989; Boore and Joyner, 1997; Avseth et al., 2001). We therefore extract the velocity values from our data at a velocity interval of 5 m/s and fit the velocities of each of the three categories using the equation:

$$v = a \times h^b$$

where  $v$  is the refraction velocity (in m/s),  $h$  is the depth below the surface (in m), and  $a$  and  $b$  are parameters derived from the best-fit process. This process yields curves that are a good approximation to the

data, with goodness-of-fit ( $R^2$ ) > 0.7 in all cases. These parameters are shown in Table 1, and the best-fit curves are shown in Figs. 6A–C. We note that these velocity curves are independent of water saturation, which can strongly influence near surface seismic velocities, especially in alluvium. The velocity of water saturated alluvium generally exceeds the speed of sound in water (~1480 m/s) but is specifically dependent on porosity, water saturation, and lithology (e.g. Mavco et al., 2009).

#### 4. Discussion

The refraction profiles (Fig. 5) provide measurements of P-wave velocities to ~200 m below the surface on average, although the actual coverage depends on the site conditions, acquisition geometry, and

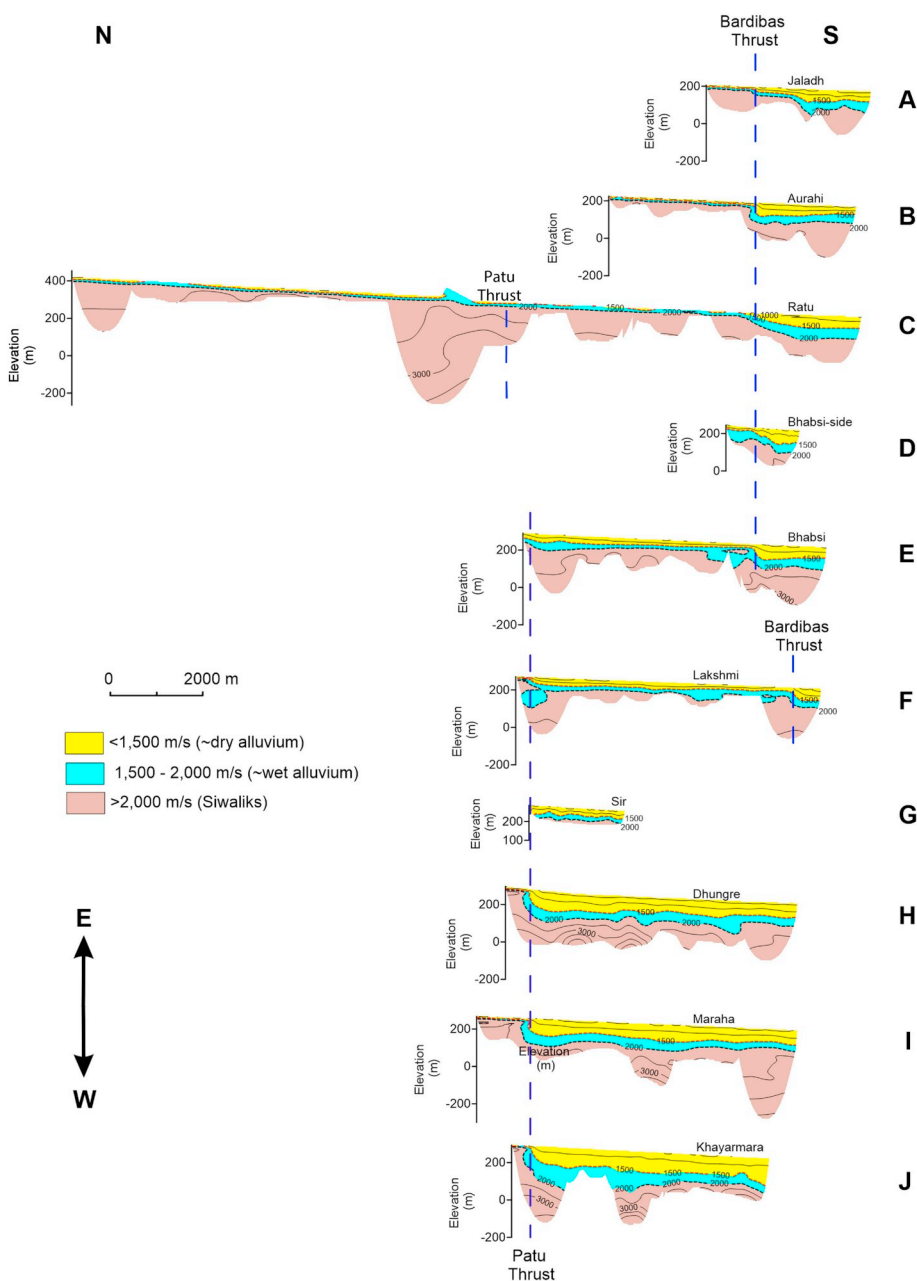


**Fig. 5.** 2D-gradient smooth velocity models with 20 to 100 WET iterations (vertical exaggeration = 4:1; vertical scale is depth in meters), generated from the seismic data collected along the ten rivers. Each contour line represent 500 m/s velocity interval. Approximate relationship between velocities and stratigraphic units are noted in the legend. (Fig. 1; (A) Jaladh (B) Aurahi (C) Ratu (D) Bhabsi-side (E) Bhabsi (F) Lakshmi (G) Sir (H) Dhungre (I) Maraha (J) Khayarmara). The vertical axis represents the elevation above sea level in meters. The yellow dashed lines overlaid on the velocity models represent the 1500 m/s boundary (~water table), while the black dashed lines represent the 2000 m/s contour, which we interpret as the contact between alluvium and the Siwaliks. The vertical dashed orange lines represent the locations of the tips of Patu and Bardibas thrusts; the sections are shifted so that these line up with each other. The seismic velocities vary from 255 to 3660 m/s, and increase with depth. There is a step-change in velocities across the thrust faults, with higher velocities in the hanging walls. (For interpretation of the references to color in this figure legend, the reader is referred to the web version of this article.)

subsurface velocity distributions. Overall, the seismic velocities vary from 255 to 3660 m/s, increasing with depth, presumably due to porosity loss with burial (e.g., Gardner et al., 1974). We note that there is a step-change in velocities across the thrust faults, with higher near-surface velocities in the hanging walls.

#### 4.1. Stratigraphy and seismic velocities

In order to characterize the relationship between depth and seismic velocity, we divide the imaged rock types into three categories: the undeformed fluvial sediment/alluvium, the Siwaliks/alluvium in the hanging wall of the Patu thrust, and the Siwaliks/alluvium in the hanging wall of the Bardibas thrust and the footwall of the Patu thrust. We cannot divide the data explicitly by stratigraphic interval because we do not have geologic cross-sections for all of the profiles and we therefore cannot correctly identify the stratigraphic interval to which each data point belongs. However, the fault divisions work as a proxy for stratigraphy because the Bardibas thrust exposes primarily Upper

Siwaliks, whereas the Patu thrust exposes a deeper section, with a significant thickness of Middle Siwaliks (Fig. 1). Hence, this division based on structure roughly correlates to the known stratigraphy.

The data show that the velocities generally increase with depth, following an approximately exponential function. This is likely primarily due to porosity loss from compaction, together with an increase due to saturation below the water table within the alluvium section (Biot, 1956). We therefore fit the three datasets with best-fit power laws, and observe that the resulting curves fit the data reasonably well (Figs. 6A-C). In the upper 250 m, which is the best-constrained region, the youngest section (undeformed sediments) exhibits the lowest velocities, while the oldest section (the Siwaliks in the hanging wall of the Patu thrust) has the highest velocities (Fig. 6D). This is expected, because the oldest rocks have been exhumed from greater depths and have experienced the highest degree of compaction, while the youngest section has been exhumed little or not at all. However, we note that the differences between the two Siwaliks curves are small, and the data coverage for the Siwaliks uplifted by the Bardibas thrust is poor.

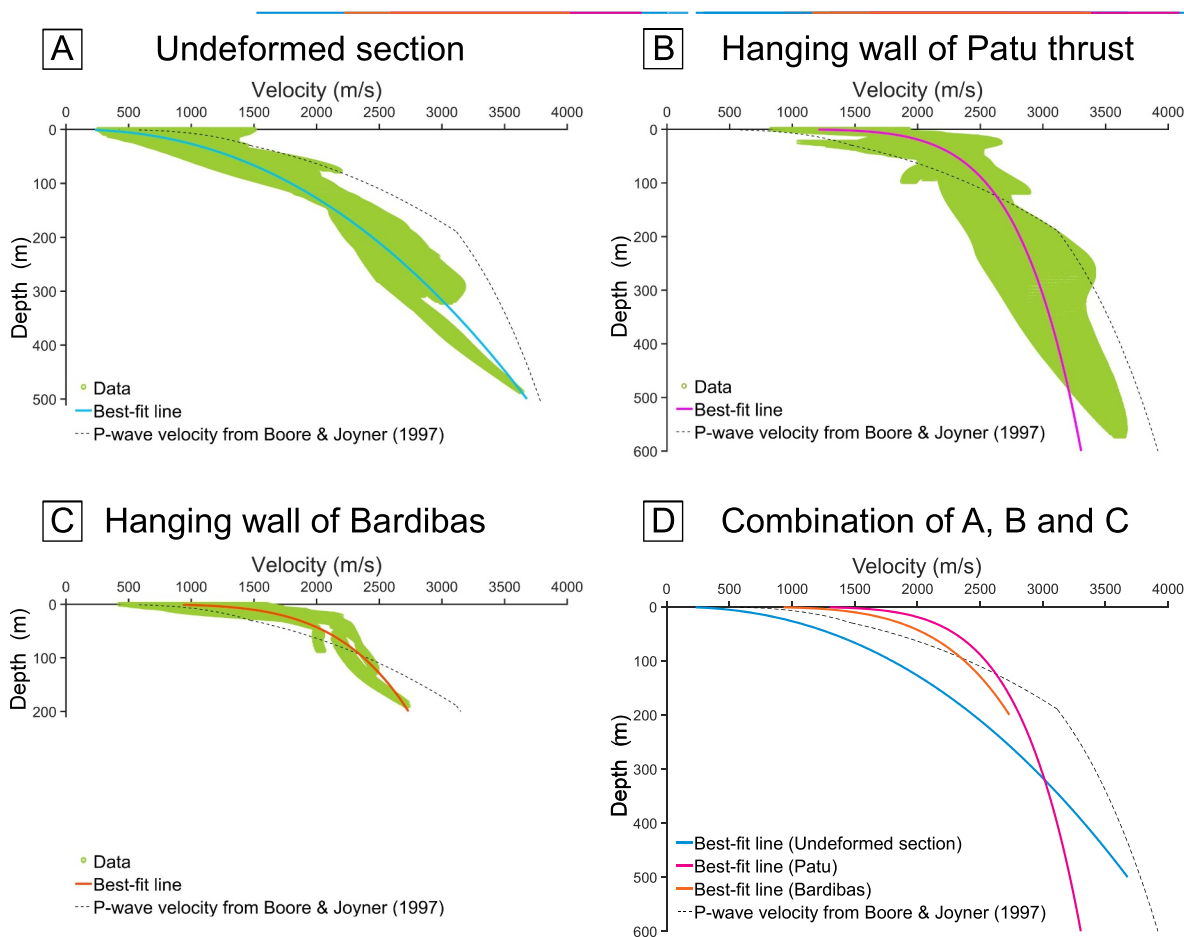


**Fig. 6.** Graph of refraction velocities vs. depth for (A) the undeformed section in the footwall of the Bardibas thrust, consisting of unconsolidated fluvial sediment, (B) the hanging wall of the Patu thrust, and (C) the hanging wall of the Bardibas thrust. (D) A comparison of all three best-fit curves. The refraction velocities of the rocks in the hanging wall of the Patu thrust are slightly faster than those at the Bardibas thrust. This is consistent with the fact that the rocks in the hanging wall of the Patu thrust were originally deeper.

At depth, the data coverage decreases, and the best-fit curves are largely constrained by shallower velocities. This is the case for the materials in the hanging wall of the Patu thrust (Fig. 6B), where the measured velocities at depths below 300 m are largely higher than the

best-fit curve. In these cases, it may be more appropriate to use different equations to model unconsolidated and consolidated strata in the appropriate depth ranges, as has been done in other studies (e.g., Boore and Joyner, 1997). For the undeformed sediment, there is relatively

**Table 1**  
Data, constants (a and b) and R<sup>2</sup> used for the best-fit curves for the three datasets.

	Number of velocity points used	Dataset included	Area of velocity model extracted		Dataset Excluded	a	b	R <sup>2</sup>
			Horizontal distance (m)	Elevation (relative to sea level, in m)				
Undeformed alluvium in the footwall of the Bardibas thrust	802,734	Ratu	15,114 to 16,849	218 to -38	Bhabsi-side (too short)	230.3	0.4454	0.9329
		Maraha	5591 to 6850	207 to -280				
		Dungre	5111 to 6234	211 to -97				
		Lakshmi	6123 to 6500	207 to -25				
		Bhabsi	5297 to 6470	225 to -96				
		Aurahi	4279 to 5285	178 to -102				
Siwaliks in the hanging wall of the Patu thrust	333,383	Jaladh	2803 to 3496	174 to -60	Bhabsi and Sir (region of hanging wall of Patu thrust is too small)	1301	0.1457	0.7740
		Ratu	6735 to 9806	313 to -259				
		Khayarmara	6 to 224	197 to 290				
		Maraha	8 to 673	142 to 260				
		Dhungre	4 to 312	236 to 285				
Siwaliks/alluvium in the hanging wall of the Bardibas thrust and the footwall of the Patu thrust	274,409	Lakshmi	3 to 242	171 to 268		887.7	0.2137	0.7078
		Ratu	10,588 to 14,082	81 to 260				
		Lakshmi	5203 to 5710	127 to 214				
		Bhabsi	3599 to 4222	194 to 237				
		Bhabsi side	0 to 159	215 to 244				
		Aurahi	7 to 222	200 to 222				
Jaladh	5 to 450	75 to 206						

little data below 350 m depth, and we therefore do not extend the curve below that level.

We correlate specific velocities with physical features based on known measurements. High porosity water-saturated sands have a P-wave velocity of about 1500 m/s (Bourbié et al., 1987; Mavco et al., 2009), and therefore we interpret that velocities greater than ~1500 m/s represent unconsolidated saturated sediments or (for velocities > 2000 m/s, as shown below) consolidated rock. In either case, we use the 1500 m/s contour as a proxy for the water table depth.

We choose 2000 m/s to represent the alluvium-Siwalik boundary. This is the velocity we observe from our profiles in the near-surface in regions where the Siwalik units crop out and the water table is high, and also consistent with Almeida et al. (2018). Published velocities for the Siwalik units in Nepal are generally higher than what we observe: between 3000 and 3400 m/s for the Upper Siwalik and 2000–3400 m/s for the Middle Siwalik (Tamrakar et al., 1999; Sarkar et al., 2012). These faster velocities are likely due to biases produced by analyzing small-scale samples (4 cm long, 2 cm in diameter) using an ultrasonic velocity measurement apparatus. For the Upper Siwalik, which is pebbly and unconsolidated, small samples will produce a bias in measurement due to the presence of pebbles and cobbles of quartzite and crystalline rocks. The bulk velocity of this unit is better measured at the scale of our seismic waves (wavelengths of 10–100 m). Note the depth step at this velocity in Fig. 6a, which represents refracted arrivals that travel along this boundary.

Using this measure of 2000 m/s, we find that the depth of the alluvium in the hanging wall of the Bardibas thrust varies between ~20–50 m and in the footwall of the Bardibas thrust it varies between ~80–120 m – i.e. about 60–70 m deeper in the footwall than in the hanging wall (Fig. 7).

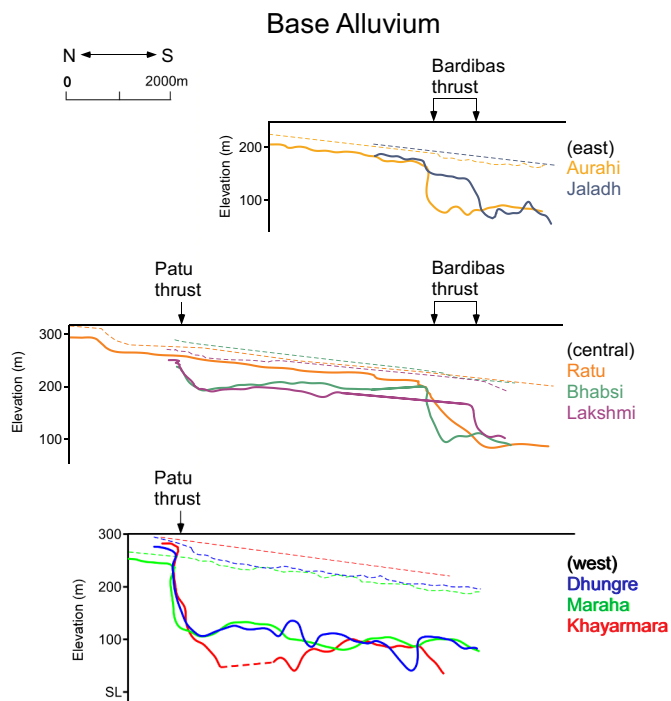


Fig. 7. Graph of depth of alluvium along the 10 river transects, with vertical exaggeration 10:1; the contours are lined up based on the locations of the faults and super-posed. The dashed lines represent the ground elevation while the solid lines represent the depth of the alluvium. In the hanging wall of the Bardibas thrust, the depth of alluvium is ~20–50 m, while in the footwall, it is ~80–120 m. The depth of alluvium decreases towards the east in the hanging wall while it remains relatively constant at the footwall of the Bardibas thrust.

## 4.2. Fault observations and their subsurface impacts

### 4.2.1. Deformation associated with the Patu thrust

Our results illuminate aspects of the subsurface tectonic deformation in this region. Seismic reflection profiles generated from our dataset (Almeida et al., 2018) show that while the Patu thrust breaches the surface, the Bardibas thrust is blind in the Ratu Khola (Fig. 2C). This result is consistent with the refraction velocity models that we present here, which show abrupt variations in the depth of alluvium. We can use this step change to map out the position of the Bardibas and Patu thrusts, as well as throw since the beginning of alluvium deposition in the hanging wall.

Four of our profiles cross the Patu thrust: the three westernmost profiles (Khayarmara, Maraha and Dhungre Kholas, Fig. H–J), as well as the Ratu Khola (Figs. 5C). The Lakshmi and Bhabsi profiles reach the Patu thrust but do not cross it far enough to have sufficient data to resolve a model in the hanging wall of the fault. Within the hanging wall, the rivers become too narrow and sinuous for effective data acquisition. In the three western profiles, we observe a single step change in the alluvium depth of ~100–170 m at the Patu thrust, with velocities that match those of the Siwaliks very close to, or at, the surface in the hanging wall, suggesting that the fault reaches the surface at these locations. Field observations indicate that at Dhungre and Maraha Kholas, the Patu thrust splits into two splays, with the more minor frontal splay raising Upper Siwaliks to the surface. Our profiles image the frontal splay.

### 4.2.2. Deformation associated with the Bardibas thrust

Where the profiles cross the Bardibas thrust, we observe a different pattern. Six lines (Figs. 5A–F) cross the Bardibas thrust, imaging its geometry for ~20 km along strike in the middle and eastern parts of our study area. In the easternmost lines (Aurahi and Jaladh Kholas; Figs. 5A,B), we observe a step change in the velocities, with Siwalik velocities near the surface in the hanging wall. However, towards the west, the pattern changes. At the Ratu Khola (Fig. 5C), where the seismic reflection data document that the fault is blind (Almeida et al., 2018), we still see Siwalik velocities in the hanging wall, but the transition zone between the footwall and hanging wall is ~150 m wide. This is consistent with the interpretation that the tip of the fault is buried and that alluvium has been deposited above the south-dipping forelimb of the fault-propagation fold imaged at greater depths by Almeida et al. (2018). These profiles show a change in depth of the alluvium of 50–100 m, with increasing throw from west to east.

West of the Ratu profile, even though there is no surface expression of the Bardibas thrust, the refraction profiles show that subsurface uplift continues for ~6 km (Figs. 5D–F). The lack of surface expression is the result of erosion of the uplifted Siwaliks and subsequent deposition of alluvial sediments in the hanging wall of the Bardibas thrust at Ratu (Almeida et al., 2018). The three westernmost profiles (Figs. 5H–J) show no step in the velocities south of the Patu thrust. This suggests that the Bardibas thrust does not exist at these locations, or has a throw that is not resolvable with our data. Furthermore, there is no indication that the Bardibas fault has stepped to the south of our profiles because the top of the Siwaliks south of the Patu thrust is not uplifted with respect to the depth of the Siwaliks in the footwall of the Bardibas thrust to the east (Fig. 7). Taken together, these profiles show how the throw on the Bardibas thrust decreases from east to west, eventually tapering to zero between the Lakshmi and Dhungre Kholas,

### 4.2.3. Soft linkage of overlapping thrust faults and slip rates

Bollinger et al. (2014) suggested that the Patu and Bardibas thrusts are hard-linked; i.e., that the Bardibas thrust curves to the north at the topographic step just west of Ratu and the two thrusts join in the subsurface (Fig. 5 of Bollinger et al., 2014). However, our refraction models indicate that instead, these faults are soft-linked (Dahlstrom, 1969; Walsh and Watterson, 1991): they overlap in map view and

presumably sole into the same décollement, while progressively transferring slip across the overlap zone. From west to east, the thickness of alluvium in the hanging wall of the Bardibas thrust decreases from ~120 m at Dhungre to 1–2 m at Ratu (according to field observations; velocity profiles indicate 10–20 m, but this is the result of smoothing by the velocity model as discussed earlier). This indicates that from west to east on the Bardibas thrust, there is an increase in throw (Fig. 5) that has occurred since the time the first alluvial sediments were deposited. In association with this, the elevation of the topography just north of the Patu thrust decreases eastward from Ratu, suggesting that slip on the Patu thrust decreases in this direction as the Bardibas thrust emerges, and that shortening is transferred between them. This soft-linkage model may represent an intermediate phase in thrust development before they become hard-linked (Davis et al., 2005; Watkins et al., 2017).

The base of the alluvium can theoretically be used as a passive marker to infer the slip rates of these thrusts. In the case of the Patu thrust, as the base of the alluvium has been completely exhumed in the hanging wall, we can only interpret a minimum rate of deformation. However, for the Bardibas thrust, the base of the alluvium remains buried across most of the profiles. If we assume that this surface formed as a beveling surface across the fault, then the step in the velocity models provides the vertical component of slip since its formation. Thus far, this surface has not been dated, but the decrease in the velocity step across the Bardibas fault towards the west allows us to qualitatively show that the fault slip and the slip rate are decreasing towards the western tip of the fault, as predicted by fault growth models (Elliott, 1976; Cowie and Scholz, 1992) and field measurements (e.g. Wilkinson et al., 2015).

#### 4.2.4. Water table

In the hanging walls of the Patu and Bardibas thrusts, the water table (1500 m/s contour) is ~10–100 m higher (Fig. 8) compared to the footwall. This is consistent with field observations: in places where the alluvium is thin in the hanging walls of the faults, the sediments at the surface are typically damp with occasional ponding, whereas in the footwalls the sediments are loose and dry. We interpret that the water table sits above the Siwaliks, in the alluvium, because the alluvium is younger and less consolidated, and therefore has higher porosity and permeability. The change in elevation of the water table is caused by uplift of the Siwaliks in the hanging wall. These conditions create a larger possible reservoir for groundwater (i.e. a greater volume of alluvium) in the footwall of the thrusts that was underfilled at the time when we acquired our data (during the dry season). During the monsoon, when the groundwater system is recharged and likely saturated, the water table is near the surface everywhere, as evidenced by the seasonal flow of the rivers where we acquired the data used in this study.

## 5. Conclusions

We use refracted waves from ten Vibroseis seismic profiles in central Nepal to generate P-wave velocity models across the Main Frontal Thrust, and use these to map the shallow subsurface down to 500 m below the surface. This dataset allows us to infer depths of water table and base of alluvium, and observe their changes across two fault strands, the Bardibas and Patu thrusts (Fig. 9). We also generate velocity-depth curves for the shallow subsurface for three distinct localities. Our main results are:

1. In general, velocities increase with depth due to compaction of the materials at depth. Since thrusting exhumes rocks that have undergone deeper burial, rocks in the hanging wall have higher velocities. Thus, the youngest undeformed section has the lowest P-wave velocities while the oldest section (Siwaliks uplifted by Patu thrust) has the highest P-wave velocities.

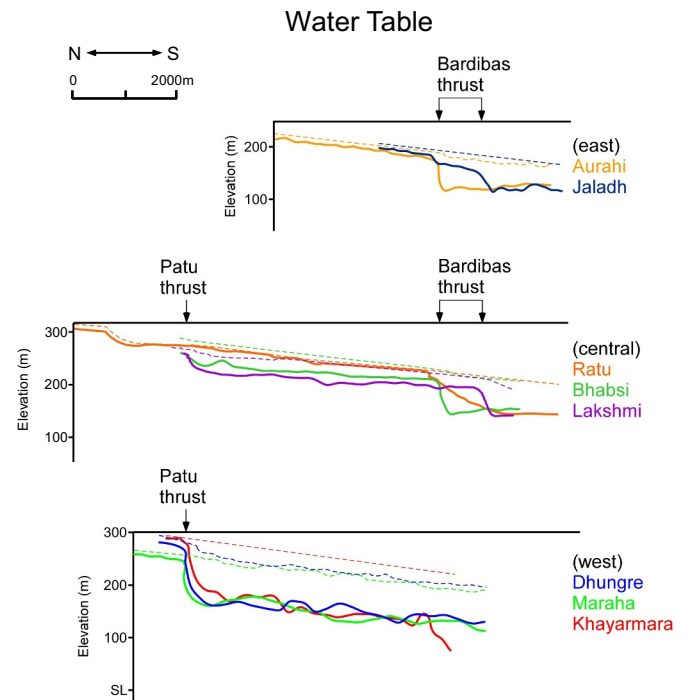
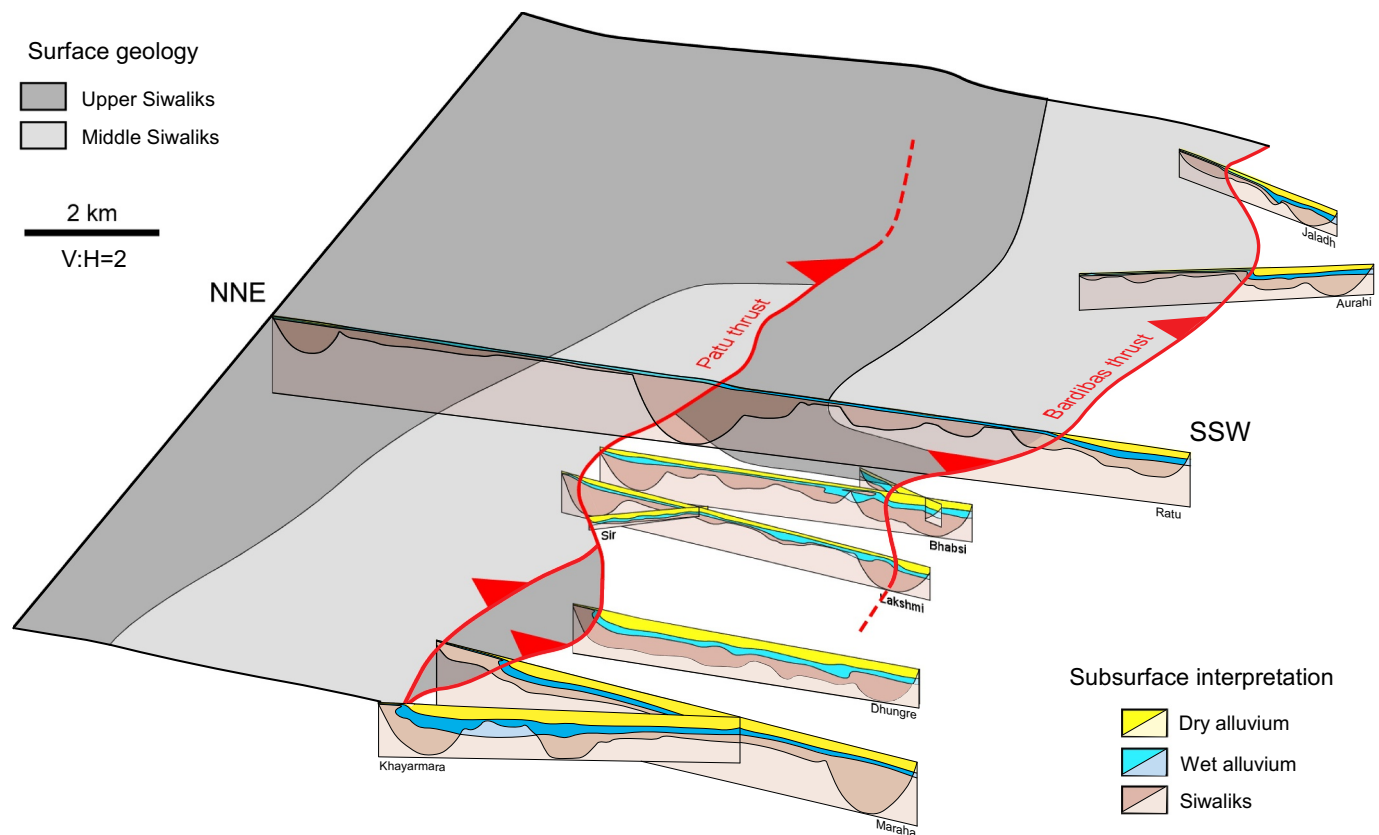


Fig. 8. Graph of depth of water table along the 10 river transects, with vertical exaggeration 10:1; the contours are lined up based on the locations of the faults and super-posed. The dashed lines represent the ground elevation while the solid lines represent the depth of the water table. In the east, the water table rises from 100 m to 2 m below the surface in the hanging wall of the Bardibas thrust, while it remains relatively constant between ~50–55 m below the surface in the footwall of the Bardibas thrust.

2. The thickness of the alluvium, as measured from velocities < 2000 m/s, varies between ~80–120 m and ~20–50 m in the footwall and hanging wall of the Bardibas thrust, respectively (i.e. about 60–70 m thicker in the footwall). This difference corresponds roughly to the amount of slip on the faults since the deposition of the fluvial sediments.

The Bardibas and Patu thrusts are soft-linked, both soling into the same décollement and transferring slip between them: slip on the Patu thrust decreases towards the east as slip on the Bardibas thrust increases. The western tip of the Bardibas thrust, where the slip tapers to zero, lies between Lakshmi and Dhungre Kholas. Thrusting has raised the less-permeable Siwalik rocks to shallow depths, therefore reducing the amount of more permeable alluvium available for groundwater storage in the region. This results in a smaller reservoir size for shallow groundwater. We show an elevated water table in the hanging walls of both the Patu and Bardibas thrusts by ~25–100 m. Our findings also confirm that in the central and western parts of our study area, the Patu thrust is surface emergent, while the Bardibas thrust is blind.

Together, these results provide detailed constraints on the fault geometries in the study area and their effect on sediment deposition and water saturation, specifically in the shallow subsurface. Bearing in mind the variability that likely occurs with seasonal precipitation, our results are relevant to hydrological studies, land-use planning and groundwater exploration. In addition, our results can be used to constrain the shallowest parts of crustal scale velocity models or in site response analyses to support seismic hazard models. Our results highlight the utility of refraction velocities, which provide constraints on subsurface features in the upper 200–500 m, supplementing surface studies (e.g. trenching, topographic analysis) and seismic reflection (which extend to 2 km but have limited resolution in the upper few hundred meters).



**Fig. 9.** Perspective view of the fault system looking towards the east. The Upper and Middle Siwaliks exposed at the surface are shown in transparent gray; the profiles are shown in the subsurface. Interpretations in profiles are extended based on general patterns, as shown in lighter colors. The Patu and Bardibas thrusts are soft-linked, i.e. the surface traces do not link and they partition shortening. The alluvium is negligible and the water table high where the Siwaliks are exposed. In the footwall of the Patu thrust west of Ratu, and in the footwall of the Bardibas thrust, the alluvium thickens and the water table deepens.

Supplementary data to this article can be found online at <https://doi.org/10.1016/j.tecto.2020.228366>.

### Funding

This work comprises Earth Observatory of Singapore contribution no. 183. This research was supported by the National Research Foundation Singapore under its Singapore NRF Fellowship scheme [National Research Fellow Award No. NRF-NRFF2013-06], and by the EOS and the National Research Foundation Singapore and the Singapore Ministry of Education under the Research Centres of Excellence initiative. We thank Landmark for donating the SeisSpace software used to process the seismic data.

### CRediT authorship contribution statement

**Yixiang Liu:**Methodology, Formal analysis, Investigation, Writing - original draft, Writing - review & editing, Visualization. **Judith Hubbard:**Conceptualization, Investigation, Resources, Writing - original draft, Writing - review & editing, Visualization, Supervision, Project administration, Funding acquisition. **Rafael Almeida:**Conceptualization, Methodology, Formal analysis, Investigation, Data curation, Writing - original draft, Writing - review & editing, Supervision, Project administration. **Anna Foster:**Methodology, Formal analysis, Investigation, Data curation, Writing - review & editing. **Lee Liberty:**Methodology, Software, Validation, Formal analysis, Investigation, Writing - review & editing, Visualization. **Ying Sin Lee:**Formal analysis, Investigation. **Soma Nath Sapkota:**Investigation, Writing - review & editing, Supervision.

### Declaration of competing interest

The authors declare that they have no known competing financial interests or personal relationships that could have appeared to influence the work reported in this paper.

### References

- Ader, T., Avouac, J., Liu-Zeng, J., Lyon-Caen, H., Bollinger, L., Galetzka, J., . . . Flouzat, M. (2012). Convergence rate across the Nepal Himalaya and interseismic coupling on the Main Himalayan Thrust: Implications for seismic hazard. *Journal of Geophysical Research: Solid Earth*, 117(B04403). doi:<https://doi.org/10.1029/2011JB009071>
- Aitchison, J.C., Ali, J.R., Davis, A.M., 2007. When and where did India and Asia collide? *J. Geophys. Res.* 112 (B5).
- Almeida, R., Hubbard, J., Liberty, L., Foster, A., Sapkota, S.N., 2018. Seismic imaging of the Main Frontal Thrust in Nepal reveals a shallow décollement and blind thrusting. *Earth Planet. Sci. Lett.* 494, 216–225.
- Avseth, P., Mavko, G., Dvorkin, J., Mukerji, T., 2001. Rock physics and seismic properties of sands and shales as a function of burial depth. In: SEG International Exposition and Annual Meeting.
- Biot, M.A., 1956. Theory of propagation of elastic waves in fluid saturated porous solid. I low frequency range, II. Higher frequency range. *J. Acoust. Soc. Am.* 28, 168–191.
- Bollinger, L., Sapkota, S.N., Tapponnier, P., Klinger, Y., Rizza, M., Van der Woerd, J., Tiwari, D.R., Pandey, R., Bitri, A., Bes de Berc, S., 2014. Estimating the return times of great Himalayan earthquakes in eastern Nepal: evidence from the Patu and Bardibas strands of the Main Frontal Thrust. *J. Geophys. Res.* 119, 7123–7163.
- Boore, D.M., Joyner, W.B., 1997. Site amplifications for generic rock sites. *Bull. Seismol. Soc. Am.* 87 (2), 327–341.
- Bouilhol, P., Jagoutz, O., Hanchar, J.M., Dudas, F.O., 2013. Dating the India-Eurasia collision through arc magmatic records. *Earth Planet. Sci. Lett.* 366, 163–175.
- Bourbié, T., Coussy, O., Zinszner, B., 1987. *Acoustics of Porous Media*. Gulf Publishing Co, Houston, Texas.
- Cowie, P.A., Scholz, C.H., 1992. Physical explanation for the displacement-length relationship of faults using a post-yield fracture mechanics model. *J. Struct. Geol.* 14 (10), 1133–1148.
- Dahlstrom, C.D., 1969. Balanced cross sections. *Can. J. Earth Sci.* 6 (4), 743–757.
- Davies, G.F., Brune, J.N., 1971. Regional and Global Fault Slip rates from Seismicity. *Nat.*

- Phys. Sci. 229 (4), 101–107.
- Davis, K., Burbank, D.W., Fisher, D., Wallace, S., Nobes, D., 2005. Thrust-fault growth and segment linkage in the active Oslter fault zone, New Zealand. *J. Struct. Geol.* 27 (8), 1528–1546.
- Dhital, M.R., 2016. *Geology of the Nepal Himalaya*, 1st edition. Springer International (498 pages).
- Eberhart-Phillips, D., Han, D.-H., Zoback, M.D., 1989. Empirical relationships among seismic velocity, porosity, and clay content in sandstone. *Geophysics* 54 (1), 82–89.
- Elliott, D., 1976. The Energy Balance and Deformation Mechanisms of Thrust Sheets. *Philos. Trans. R. Soc. A Math. Phys. Eng. Sci.* 283 (1312), 289–312.
- Faust, L.Y., 1951. Seismic velocity as a function of depth and geologic time. *Geophysics* 16 (2), 192–206.
- Gardner, G.H., Gardner, L.W., Gregory, A.R., 1974. Formation velocity and density—the diagnostic basics for stratigraphic traps. *Geophysics* 39 (6), 770–780.
- Jansen, Stefan, 2011. *Parameter Investigation for Subsurface Tomography with Refraction Seismic Data*. Master Thesis. University of Copenhagen.
- Khan, S.D., Walker, D.J., Hall, S.A., Burke, K.C., Shah, M.T., Stockli, L., 2009. Did the Kohistan-Ladakh island arc collide first with India? *Geol. Soc. Am. Bull.* 121 (3–4), 366–384.
- Larson, K.M., Bürgmann, R., Bilham, R., Freymueller, J.T., 1999. Kinematics of the India-Eurasia collision zone from GPS measurements. *Journal of Geophysical Research: Solid Earth* 104 (B1), 1077–1093.
- Lave, J., Yule, D., Sapkota, S., Basant, K., Madden, C., Attal, M., Pandey, R., 2005. Evidence for a Great medieval earthquake (~1100 A.D.) in the Central Himalayas, Nepal. *Science* 307 (5713), 1302–1305.
- Mavco, G., Mukerji, T., Dvorkin, J., 2009. *The Rock Physics Handbook: Tools for Seismic Analysis of Porous Media*. Cambridge University Press.
- Sapkota, S.N., Bollinger, L., Klinger, Y., Tapponnier, P., Gaudemer, Y., Tiwari, D., 2013. Primary surface ruptures of the great Himalayan earthquakes in 1934 and 1255. *Nat. Geosci.* 6, 71–76.
- Sarkar, K., Vishal, V., Singh, T.N., 2012. An empirical correlation of index geomechanical parameters with the compressional wave velocity. *Geotech. Geol. Eng.* 30 (2), 469–479.
- Schuster, G.T., Quintus-Bosz, A., 1993. Wavepath eikonal traveltimes inversion: theory. *Geophysics* 58 (9), 1314–1323.
- Sheehan, J.R., Doll, W.E., Mandell, W.A., 2005. An evaluation of methods and available software for seismic refraction tomography analysis. *Journal of Environmental & Engineering Geophysics* 10 (1), 21–34.
- Tamrakar, N.K., Yokota, S., Nakamura, M., 1999. Some mechanical properties of the Siwalik sandstones and their relation to petrographic properties. *Shimane Univ. Environmental Science Report* 18, 41–54.
- Walsh, J.J., Watterson, J., 1991. Geometric and kinematic coherence and scale effects in normal fault systems. In: Roberts, A.M., Yielding, G., Freeman, B. (Eds.), *The Geometry of Normal Faults*. Geological Society of London Special Publication 56. pp. 193–206.
- Watkins, H., Butler, R.W., Bond, C.E., 2017. Using laterally compatible cross sections to infer fault growth and linkage models in foreland thrust belts. *J. Struct. Geol.* 96, 102–117.
- Wilkinson, M., et al., 2015. Slip distributions on active normal faults measured from LiDAR and field mapping of geomorphic offsets: an example from LAquila, Italy, and implications for modelling seismic moment release. *Geomorphology* 237, 130–141.
- Yilmaz, Ö., 2001. *Seismic Data Analysis*. Society of Exploration Geophysics 2065 pages.